ACS APPLIED MATERIALS & INTERFACES

Research Article

www.acsami.org

Sustainable Polyelectrolyte Multilayer Surfaces: Possible Matrix for Salt/Dye Separation

Akhil Gopalakrishnan,[†] Mary Lidiya Mathew,[†,§] Jisha Chandran,[‡] Judith Winglee,[⊥] Appala Raju Badireddy,[⊥] Mark Wiesner,*[,⊥] Charuvila T. Aravindakumar,[‡,∇] and Usha K. Aravind*[,†,§]

[†]Advanced Centre of Environmental Studies and Sustainable Development, [‡]Inter University Instrumentation Centre, and [∇]School of Environmental Sciences, Mahatma Gandhi University, P.D. Hills P.O., 686560 Kottayam, India

[§]Centre for Environment Education and Technology (CEET), Kiranam, Arpookara East P.O., 686008 Kottayam, India

[⊥] Center for Environmental Implications of Nano Technology (CEINT), Duke University, Box 90287, 121 Hudson Hall, Durham, North Carolina 27708-0287, United States

Supporting Information

ABSTRACT: The development of a sustainable membrane surface based on chitosan/poly(acrylic acid) (CHI/PAA) multilayers suitable for applications in analytical separations is reported here. Bilayers are constructed on polyamide microfiltration membranes at a pH combination of 3/3 (CHI pH/PAA pH) through a layer by layer approach. A 12.5 bilayer yielded a thickness of 400 nm. Low pressure (10 psi) filtrations through a 5.5 bilayered membrane exhibited high flux (7 m^3 m^{-2} day^{-1}) and selectivity (NaCl/reactive black 5 (RB5) selectivity >8000). The selectivity and flux observed here are the highest reported to date for low pressure filtrations through membranes. The increase in flux with increasing feed salt concentration is correlated with morphological transformations. Salt content above 7500 ppm causes some perturbation of surface layers. The presence of RB5, a model dye in the feed, restores the surface to maintain sustainability. A skin layer as thin as 50 nm imparts a large separation window. An RB5 feed concentration of 500 ppm results in 98.64% rejection with a flux of 25.79 m^3 m^{-2} day^{-1}. The increase in flux with feed dye concentration supports the plasticizing action of RB5. The transport studies with large feed dye concentrations indicate that at a dye concentration of 500 ppm, the linear growing region (pre-exponential, 5.5 bilayer) itself provides a separation window similar to that of 100 ppm. At the same time, 1000 ppm requires a 9.5 bilayer that falls in the nonlinear growing region. Scanning electron microscopy images show the increase in porosity with respect to feed dye. Interesting morphologies that show the sustainable nature of the membrane surfaces along with the transport data of RB5 are presented.

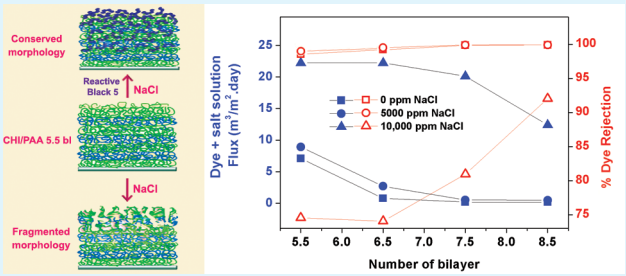

KEYWORDS: *layer by layer assembly, multilayer films, morphology, microporous membranes, sustainable surface*

INTRODUCTION

Textile effluent is one of the primary contributors to water pollution. The major challenge facing waste treatment plants of textile industries is the complete removal of color with no trace of organic dyes getting discharged into the water supply. Technologies that can provide recyclable water free from dyes and salts may provide a substantial reduction in fresh water consumption and over burden of dye usage. In spite of new techniques, textile effluents often carry residual dyes, salts (either added or as an impurity along with the dye), and many other chemicals from the dyeing process.[1−3] This discharge creates an intense color[3,4] and a high chemical and biological oxygen demand.[2,5−7] Reactive dyes are highly colored water-soluble anionic compounds with a high fasting capacity and low fixation rate that are widely used in cotton and rayon. These dyes, when applied to fiber, form covalent bonds with hydroxyl groups on the cellulose fibers.[1,2,8] They also have the highest discharge (∼50%) share of the different dye classes.[2,3] High levels of salt that are present in the effluent are another cause of concern. The resistance of the dyes to degradation by sunlight, microorganisms, and oxidizing agents forces them to become an integral part of the ecosystem, resulting in an alarming situation. Conventional wastewater treatment plants utilize techniques like sorption[2] and aerobic biodegradation[9] for dye removal, which are almost impracticable for reactive dyes. This leads to the situation of effluents with high color even when the dye concentration is in the range of 10−50 ppm.[3]

Membrane-based separation processes are widely employed for the treatment of dye-based effluents.[1,5] Particularly, pressure-driven membrane processes show steady growth in this sector. The major setbacks have been fouling and the high pressure required at various separation stages. Advances in

Received: November 26, 2014
Accepted: January 23, 2015
Published: January 23, 2015

DOI: 10.1021/am508298d
ACS Appl. Mater. Interfaces 2015, 7, 3699−3707

surface coating methods enable specially designed skins in composite membranes that can largely address both of these issues.[10]

A layer by layer (LbL) approach is perhaps the most suitable method for designing separation skin in composite membranes. The flexibility of the skin in its morphology, thickness, and permeation characteristics is not restricted to simply the availability of materials[11,12] but to pre- and posttreatment options.[13−17] LbL assembly can in fact be realized from various materials that have alternately charged groups. However, using polyelectrolytes as a depositing species has its own merits for designing membrane surfaces for applications related to separations. The conformation of polyelectrolytes responds easily to changes in pH[18,19] and ionic strength.[13,17,20] This allows for precise control of the film's architecture. An added advantage of such a skin is its reversibility through its well-studied open and closed shell behavior.[21] After Decher et al.[22] introduced LbL assembly of polyelectrolytes, this method was adapted extensively for the generation of nanostructures. This approach involves the sequential adsorption of oppositely charged polyelectrolytes on a charged porous substrate. There is a surface charge reversal in each step that enables deposition of the next layer. The environmental friendliness of LbL is an added advantage that makes this robust method an unparalleled tool for the surface modification of membranes. However, gaps still exist when one considers the industrial application side of the LbL approach for generating new materials. The development of porous materials with controllable features to go well with a particular application is always a challenging problem. The primary focus for microporous membranes has been the development of drug delivery applications.[23−26] To date, not enough attention has been paid to the usage of these membrane materials for industrial water treatment.

LbL-coated surfaces are particularly interesting because of their tunable growth trends (linear/exponential) and the possibility of external doping. These two properties may positively contribute to maintaining sustainability in real time filtrations. Sustainable surfaces are plentiful in nature[27,28] and are maintained through self-repair mechanisms. Attempts to bestow the property of sustainability through self-healing onto synthetic materials are ongoing constantly.[29,30] Both intrinsic and extrinsic self-repair mechanisms are found to be operative in LbL coatings.[29,31,32] Self-healing has been found to take place in exponential regions where interdiffusing polymer chains are plentiful.[31] To the best of our knowledge, no reports have addressed re-formations that take place in a multilayer with only a few bilayers of coating when they are still in the linear growing region. Thus, the possibility of forming sustainable surfaces that are very thin and provide a large flux at low pressure filtrations are addressed in this paper.

Chitosan, one of the most popular linear polysaccharides and a polycation, is expected to provide an interesting skin for dye/salt separations considering the availability of sites for primary and secondary interactions, such as electrostatic forces, van der Waals interactions, and hydrogen bonding. A few earlier studies on the chitosan/poly(acrylic acid) (CHI/PAA) multilayer system had different dimensions regarding its application. Chen et al.[33] utilized the CHI/PAA multilayer coated on magnetic Fe_3O_4 microspheres for the removal of the cationic dyes methylene blue (MB) and crystal violet. A large mass gain for the same multilayers on quartz crystals and silicon wafer substrates at a pH combination of 5/2.7 was also reported,[26] and drug delivery applications were explored. Our group has previously studied the effectiveness of the same bilayer system for dye removal (coomassie brilliant blue (CBB) and MB) under adsorption conditions.[5] In the present study, the nano separation skin is fabricated from CHI and PAA on a nylon 6,6 microfiltration membrane support. A suitable deposition pH is optimized for both polyions under which they exhibited linear growth at a lower number and nonlinear growth at a higher number of layers (>6.5). The transport profile of NaCl/RB5 is discussed at varying numbers of bilayers and salt/dye concentrations under low pressure filtration. The invariable presence of salt in wastewater generated by the dye industry (especially textile mill effluent) is taken into account when determining the exposure concentration of sodium chloride (NaCl). The respective morphological features at linear and nonlinear growing regions are reported together with desorption information.

EXPERIMENTAL SECTION

Materials. Ultipor N66 (nylon 6,6; 0.45 μm pore diameter; uncharged) and Supor450 (polyether sulfone; 0.45 μm pore diameter) microfiltration membranes purchased from the Pall Corporation were used as support membranes of multilayer formation for transport studies. Silicon wafers with one polished side and [100] orientation were used as substrates for multilayer formation thickness measurements. Chitosan (medium molecular weight, 75−85% deacetylated, Sigma-Aldrich), poly(acrylic acid) sodium salt (MW 30000, 45 wt % aqueous solution, Sigma-Aldrich), reactive black 5 (MW 991.82, Sigma-Aldrich), citric acid (Qualigens), sodium citrate dehydrate (Ranbaxy), and sodium chloride (Merck) were used without further purification. Ultrapure water (18.2 MΩ cm) obtained from a Cascada AN water purifying system (Pall Corporation) was used for all experiments.

Preparation of a Multilayer Using the Layer by Layer (LbL) Technique. Multilayers were prepared from 0.01 M polyelectrolyte solutions. The polyelectrolyte concentration was calculated on a repeating unit basis. To dissolve CHI in water, diluted HCl was used instead of acetic acid to avoid the presence of acetate ions in the system.[34,35] Complete dissolution of CHI was not achieved above pH 3 when HCl was used alone.[34] The aqueous solutions of CHI and PAA were carefully adjusted to the required pH using 1 M HCl and a calibrated pH meter. The pH of CHI was adjusted to within a range from 1.72 to 3 and that of PAA from 2 to 5. The support membranes were kept in water overnight before multilayer preparation. LbL deposition was initiated by keeping the support membrane in CHI solution for 15 min. The membrane was then taken out and washed twice with deionized water to remove loosely bound polyelectrolytes. It was then placed in PAA solution for another 15 min and washed. Thus, a layer of a pair of oppositely charged polyelectrolyte was formed, which is termed one bilayer. This cycle was repeated until the desired number of bilayers was obtained. A system with "*n*" number of bilayers is designated as a CHI/PPA *n* bilayer. A multilayer with *n* bilayers that is terminated with one additional layer of CHI is represented as a CHI/PAA *n*.5 bilayer.

For thickness measurements of multilayers using spectroscopic ellipsometry, silicon wafers were used as the substrates. They were sonicated for 15 min in deionized water and then treated in a 1:7 mixture of H_2O_2/H_2SO_4 at 80 °C for 20 min. The wafers were then washed several times, dipped in a 1:1:5 mixture of H_2O_2/NH_4OH/water at 70 °C for 15 min, and washed several times. These wafers were kept in deionized water and used immediately for the LbL deposition of polyelectrolytes using the same procedure described for polymer supports.

Membrane Characterization. *Attenuated Total Reflectance Fourier Transform Infrared (ATR-FTIR) Spectroscopy.* Polyelectrolyte multilayer buildup was characterized by FTIR analysis using a Shimadzu IR Prestige-21 spectrophotometer. The absorption spectra were recorded from 650 to 4000 cm^{-1} using an ATR attachment with a ZnSe crystal. Twenty scans were averaged per spectrum. The relative

DOI: 10.1021/am508298d
ACS Appl. Mater. Interfaces 2015, 7, 3699−3707

changes in the carbonyl stretching frequencies of the carboxylic acid and carboxylate groups (1716 and 1500−1580 cm^{-1}, respectively) of PAA in the multilayer were used for monitoring multilayer formation and modification.

Spectroscopic Ellipsometry. The thickness of the multilayers was measured using a spectroscopic rotating compensator ellipsometer (M-2000V, J. A. Woollam Co.) in the wavelength range of 370−1000 nm at angles of incidence of 65, 70, and 75° and at three different locations on the sample. Spectroscopic ellipsometers can measure thicknesses of a few micrometers using near-infrared light. Silicon wafers have a natural SiO_2 coating with a thickness of ∼2 nm that was determined prior to multilayer preparation. Optical modeling and data analysis were performed using Complete EASE software, version 4.81 (J. A. Woollam Co.). A three layer optical model consisting of Si-substrate/SiO_2/polyelectrolyte multilayer was used. The polyelectrolyte multilayer was modeled as a single homogeneous B-spline layer with a refractive index that was assumed to be 1.5.

Scanning Electron Microscope (SEM). Surface morphologies of unmodified and modified membranes were imaged using a Philips FEI XL30 SEM with a field emission gun (FEG).

Low Pressure Filtration Studies. Filtration experiments were performed in an Amicon 8050 dead-end stirred cell with a total volume of 50 mL and an effective membrane area of 13.4 cm^2. Filtration was performed under a constant N_2 pressure of 10 psi with continuous stirring at a rate of 300−400 rpm at room temperature. Solutions of reactive dyes were prepared with varying amounts of NaCl and a fixed dye concentration of 100 ppm unless otherwise specified. The solution was buffered to pH 3 and then homogenized by stirring continuously with a magnetic stirrer under heating at 60 °C for 1 h. The concentration of the reactive dye in the feed and permeate was measured using a UV-Vis spectrophotometer (PerkinElmer Lambda 650). The percentage of permeated salt was determined by measuring the concentration of chloride ions in the feed and the permeate through an ion chromatograph (Dionex ICS-1100 IonPac AS12A column, Onguard II RP cartridges, and a conductivity detector). Flux was calculated using eq 1, where V is the volume of permeate collected, A is the effective membrane area, and Δt is the permeation time.[36]

$$J = \frac{V}{A\Delta t} \quad (1)$$

RESULTS AND DISCUSSION

Growth Pattern of Bilayers. The development of a nanoskinned microfiltration membrane was initiated by alternating layer by layer deposition of CHI and PAA. CHI, a natural polysaccharide, is very economical as a polycation for industrial purposes due to the abundance of its precursor chitin. Combination of the weak polyelectrolyte CHI with the weak polyanion PAA makes for a pH-tunable system from the perspective of the thickness of a bilayer, which is the fundamental unit of a multilayer. The critical factor that decides the thickness and interpenetration of the neighboring layers in weak polyelectrolyte pairs is the degree of ionization, which is in turn controlled by the pH of the deposition. In the present system, the deposition for a multilayer is examined for CHI (pK_a ∼ 6.0) at acidic pH in the range 1.7−3 and for PAA (pK_a ∼ 4.8) in the range 2−5. The pK_a value of the polyelectrolyte depends on the environment, and thus in going from a solution to solid state (in the multilayer film) the degree of ionization may change. Several pH combinations of both polyelectrolytes were determined to generate a thick skin layer. In our previous studies, we demonstrated that the acidic deposition pH of 1.7−1.8 for a chitosan−poly(styrenesulfonate) multilayer was effective in separating various medium to large molecular weight dyes and proteins.[5,37−39] Thus, this acidic pH range was chosen as the deposition pH for the present system. The pH of CHI was varied from 1.7 to 3, and the pH of the PAA solution was varied from 2 to 5. The infrared absorbance of a CHI/PAA 5 bilayer prepared in the selected deposition pH range is presented in Figure 1. Because

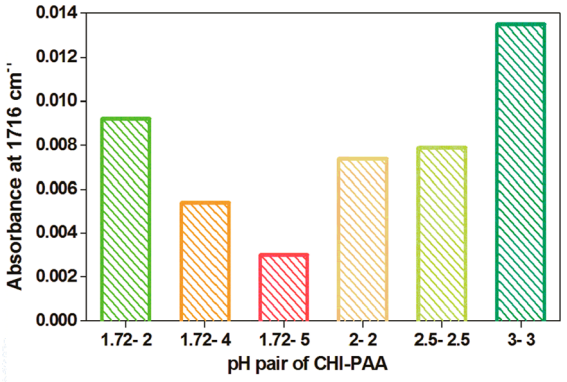

Figure 1. Variation in IR absorbance of the carboxylic acid group (C═O stretching at 1716 cm^{-1}) as a function of pH of a CHI/PAA 5 bilayer on a nylon 6,6 support membrane.

the absorption peak of nylon in the carboxylate region (1500−1570 cm^{-1}) supports membrane overlap, the carboxylic acid peak was taken at 1716 cm^{-1} as the indicator band, as this region is free from substrate influence. The carboxylic acid peak showed maximum intensity with the pH 1.72/2 (CHI pH/PAA pH) combination. In other combinations, both polyelectrolytes were maintained at similar pH 2/2, 2.5/2.5, and 3/3 combinations. The growth patterns are shown in Figure 1. The absorbance and hence the thickness were observed to be highest at pH 3/3 among all the combinations studied.

In the FTIR spectra, because the nylon peak overlaps the carboxylate region, it is very difficult to determine the ionization of PAA. To overcome this difficulty, we deposited the bilayers under the same conditions on a polyether sulfone support membrane, for which the infrared absorption is less pronounced compared to that of nylon 6,6 in the carboxylate region. The corresponding ATR spectra are presented in Figure 2.

PAA was expected to give low ionization at the selected lower pH range of 2−3 because of its higher solution pK_a value of 4.8.[26] Surprisingly, PAA is ionized to a significant extent at lower pH values. It is known that the pK_a of a weak polyelectrolyte is sensitive to its local environment. The degree of ionization of a polyelectrolyte in a multilayer depends on several factors.[40,41] The addition of the polycation to PAA brings the pK_a of PAA down to a lower value, which in turn induces ionization of non-ionized PAA segments. This fact was discussed by Rubner and co-workers in their study of PAA opposite of PAH, PDAC, or PVTAC, where the degree of ionization was significantly different from that of the solution state.[18,42] The change was more prominent in the PAA/PAH pair. In combination with PAH, even at pH 2, PAA was significantly ionized. Local ionization and pH are controlled by the distribution of ions, which in turn is influenced by the local electric field in the vicinity.[43] Thus, during the deposition process, the ionization of a polyelectrolyte in solution near the multilayer surface will differ from its ionization in the bulk of the solution. Therefore, if the surface potential is negative (top layer of PAA in the present case), protons are enriched near the surface, which means the pH at the surface is lower than that in

DOI: 10.1021/am508298d
ACS Appl. Mater. Interfaces 2015, 7, 3699−3707

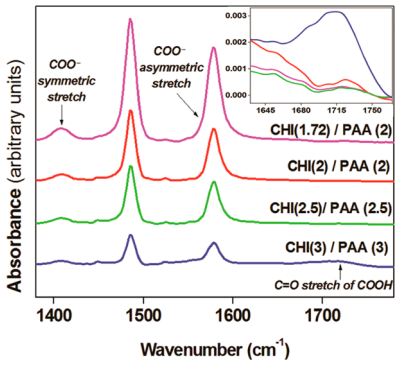

Figure 2. FTIR spectra of a CHI/PAA 5.5 bilayer membrane deposited on a polyether sulfone support from polyelectrolyte solutions of various pH 1.72/2, 2/2, 2.5/2.5, and 3/3 combinations. The pH of the respective deposition solution is shown in parenthesis. Spectra are stacked at an arbitrary offset for clarity. Inset shows overlaid spectra of the same set of data to illustrate the difference in absorbance of the C═O stretching frequency of the COOH group in the 1630−1770 cm^{-1} region. The maximum absorbance in this region is shown by a CHI/PAA multilayer deposited at pH 3/3.

the bulk; conversely, the pH at the surface is higher if the surface potential is positive (top layer of CHI in the present case). This in turn could affect the degree of ionization of the new adsorbed layer. In the present system, the ionization is found to depend on the charge of the opposite polyelectrolyte.[44] At the lower pH of 1.72, CHI is highly positively charged with entire amine groups existing as NH_3^+, which perhaps influences the dissociation of the carboxylic acid group, whereas at pH 3, the degree of ionization of CHI drops slightly and PAA is almost 78% ionized, resulting in a thicker film. The degree of ionization was calculated (see Supporting Information, Table S1) based on an equation reported elsewhere.[45] Dissimilarity in the deposition pHs (i.e., 2/4 or 2/5) resulted in thinner layers. Here, the degree of ionization of PAA in turn influences the charge on CHI, which meanas both may have the unfavorable situation of partial ionization preventing the production of thick layers.[26]

The bilayer-dependent growth pattern at pH 3/3 was further analyzed by spectroscopic ellipsometry, and the results are presented in Figure 3A. The plot indicates linear growth at a lower number of bilayers followed by a nonlinear region. Nonlinear growth is generally attributed to in and out diffusion of one or both of the polyelectrolytes involved.[46] Even so, there

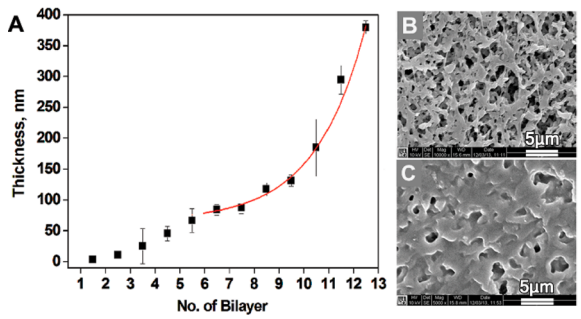

Figure 3. (A) Nonlinear growth of the CHI/PAA multilayer membrane with deposition steps measured using spectroscopic ellipsometry. The solid line shows the exponential fit for the CHI/PAA multilayer. (B) SEM images of a CHI/PAA 2.5 bilayer and (C) a CHI/PAA 9.5 bilayer.

are reports that nonlinear growth can be recognized to arise from the particular conformation and charge density of polyelectrolyte chains at given assembly conditions.[47,48] From Figure 3B and C, it can also be seen that beyond 8.5 bilayers, the mass gain is very high. The multilayer skin gains a large thickness (~380 nm) within 12 bilayers.

The morphological changes in the membrane upon multilayer growth can be seen in the SEM images (Figure 3). The increment in polyelectrolyte deposition is clearly observable at the CHI/PAA 2.5 bilayer. The mass deposited increases with each layer coated, which in turn reduces the porosity. Ellipsometric measurements at a higher number of deposited layers showed nonlinear growth. The number of polyelectrolytes deposited at a 9.5 bilayer (Figure 3C) is so high that pores are getting partially covered. The surface roughness is also found to increase with the number of deposited layers. A study by Liu et al.[49] on CHI/PAA multilayers pointed out that the multilayer consists of islands that grow during the buildup process, leading to a nearly exponential increase in the roughness with the number of bilayers added. Here, it can also be assumed that the islandlike morphology and subsequent increase in roughness contribute to the nonlinear growth.

To examine the suitability of CHI/PAA membranes in the isolation of organic dyes from aqueous and salt solutions, RB5 was filtered under low pressure driven conditions (10 psi) through a varying number of bilayers. The results of this process are presented in Table 1.

Table 1. Transport Characteristics of RB5 (100 ppm) through a CHI/PAA Multilayer as a Function of the Number of Bilayers

number of bilayers	NaCl feed concentration (ppm)	flux $m^3\ m^{-2}\ day^{-1}$	dye rejection (%)
5.5		7.08	99.99 ± 0.01
6.5		0.77	99.98 ± 0.02
5.5	5000	8.90	99.99 ± 0.01
6.5	5000	2.69	99.80 ± 0.03
5.5	10000	22.23	74.56 ± 0.10
6.5	10000	23.88	80.94 ± 0.08

The results clearly indicate that within a few bilayers high rejection is observed. In previous work with CHI/PAA under adsorption conditions, uptake of dye was found to be very dependent on the type of bilayers. Alkaline effluent pH resulted in 79.9% MB and 87.1% CBB removal with 20 bilayers. Shifting the buildup pH as discussed above resulted in a positive difference in terms of the percentage of dye removal and flux. A few bilayers could impart complete recovery (HPLC chromatogram shown in Supporting Information, Figure S1) of dye under a low pressure driven condition. A multilayer coating of 2.5 bilayers (~4.8 nm) itself is able to remove ~70% of the dye (Supporting Information, Figure S2), which increases to 99.84% with very high flux (7.08 $m^3\ m^{-2}\ day^{-1}$) at 5.5 bilayer (~66.6 nm). Optical images of the multilayers used for dye removal are shown in Figure 4.

Industrial effluents often carry a large amount of salt, and separations would be more meaningful if the salt could be separated into the permeate as well. Commercial membranes do not provide a good separation window. From this perspective, performance improvement has been found for PSS/PAH membranes on an alumina support (0.02 μm Whatman Anodisk filters) as reported by Bruening et al.[10]

DOI: 10.1021/am508298d
ACS Appl. Mater. Interfaces 2015, 7, 3699−3707

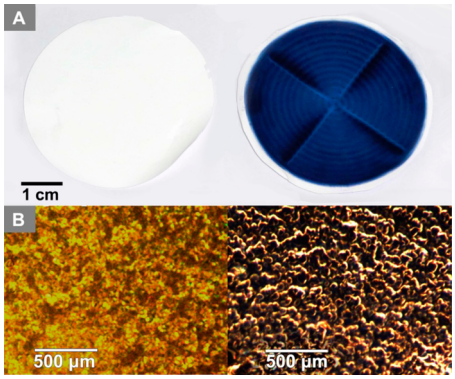

Figure 4. Optical images of a CHI/PAA 5.5 bilayer membrane before (left) and after (right) filtration of 100 ppm RB5. (A) Digital photographs and (B) enhanced darkfield transmission optical microscope images.

Very high rejection for RB5 (1000 ppm) with a reasonable flux of 1.7 m^3 m^{-2} day^{-1} was achieved by this membrane at an operating pressure of 4.8 bar.

As shown in Table 1, a salt content of 5000 ppm in the feed resulted in 99.9% rejection of RB5 with a flux of 8.9 m^3 m^{-2} day^{-1}. The flux value further increased to 22.23 m^3 m^{-2} day^{-1} at a salt content of 10000 ppm. The rejection value decreased, and additional coating was necessary to improve the rejection. The higher flux values observed in the presence of salt content in the feed indicate possible morphological changes of the membranes. To better understand these changes, we filtered salt solutions of different ionic strengths (2500−15000 ppm NaCl) through the CHI/PAA membranes at 5.5 bilayers. The transport properties were monitored with respect to the feed salt concentration as shown in Figure 5. An initial addition of

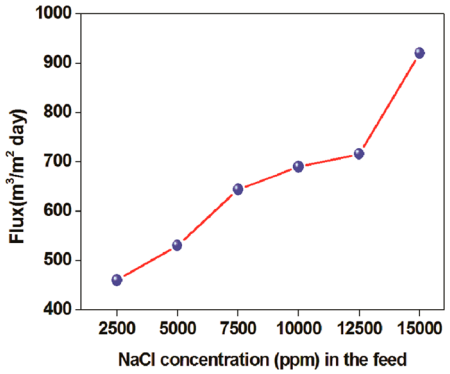

Figure 5. Variation of flux through a CHI/PAA 5.5 bilayer with salt concentration varying from 2500 to 15000 ppm in the feed solution.

2500 ppm salt increased the flux to 460.54 m^3 m^{-2} day^{-1}. The flux was found to further increase with increased salt concentration in the feed. The increase in the flux shows a nonlinear pattern. The graph shows a linear nature up to a concentration of 7500 ppm and thereafter shows a slight negative deviation. A high concentration of feed salt, 15000 ppm, resulted in an abrupt rise in flux. This clearly suggests that the membrane structure is altered based on the ionic strength of the contact solution, that the structural modification is uneven, and that it is more distinct above a salt concentration of 7500 ppm.

Exposure to monovalent electrolytes at a modest concentration itself may induce morphological transformation in the current polyelectrolyte pair because the polyions involved have amino and carboxyl functional groups. The unexposed CHI/PAA 5.5 bilayer (Figure 6A) features a porous topography that

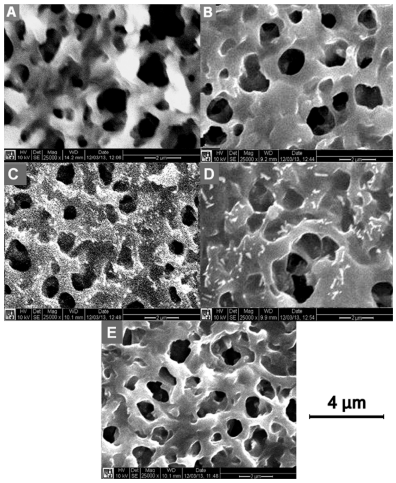

Figure 6. SEM images of CHI/PAA 5.5 bilayer membranes before filtration (A) and after filtration with a feed solution of 2500 (B), 7500 (C), and 15000 ppm (D) NaCl and after filtration with a 7500 ppm NaCl solution containing 100 ppm RB5 (E).

is clearly distinguishable from the underlying substrate. At an electrolyte concentration of 2500 ppm, the surface of the film gets smoother with a transformation from fuzzy irregular pores to distinct round pores (Figure 6B). However, the number of pores increases, which is clearly visible in the SEM image (Supporting Information, Figure S3). In fact, in polyelectrolyte multilayers, the surface roughness is reduced by the annealing of salt.[13] The softening property depends on the functional groups and the hydrophilic nature of the polyion pairs. The onset of smoothing differs for different polyion pairs. For instance, PAA/PAH[50] requires higher salt concentrations to produce the same effects obtained with the CHI/PAA pair. Another factor that supports smoothing is the rearrangement of polyelectrolyte pairs to equilibrate the free energy distribution. This happens in the presence of an external dopant such as NaCl. In the multilayered state, polyion pairs are intrinsically compensated by reversible electrostatic cross-links. However, the dopant induces breakage of these cross-links to introduce ion exchange sites (eq 2). Apparently, the breaking of the polyelectrolyte chains is enough to produce a more porous matrix, which accounts for the increase in flux. The increase in pore diameter obtained from the SEM images (Supporting Information, Table S2) also substantiates an increasing flux pattern at higher salt concentrations.

$$\mathrm{Pol^+Pol^-_{(m)}} + \mathrm{Cl^-_{(aq)}} + \mathrm{Na^+_{(aq)}} \rightleftharpoons \mathrm{Pol^+Cl^-_{(m)}} + \mathrm{Pol^-Na^+_{(m)}} \quad (2)$$

where Pol^+ and Pol^- represent CHI and PAA repeating units, respectively, and the subscripts m and aq refer to the multilayer and aqueous phases, respectively.

Further addition of salt to a concentration of 5000 ppm showed a linear increase in flux, which agrees exactly with the values observed in Table 1. A salt content of 7500 ppm induced a deviation in the linear pattern of flux. The SEM image

DOI: 10.1021/am508298d
ACS Appl. Mater. Interfaces 2015, 7, 3699−3707

presents a distorted surface morphology (Figure 6C) with the appearance of small domain features. A close look at the images reveals the appearance of a broken network at the surface layer. Flux values remain steady up to a salt concentration of 12500 ppm. A further increment in stress appears to have resulted in the formation of a polyelectrolyte complex that may separate out. At a salt concentration of 15000 ppm, the multilayer further loosens with enhanced perturbation. The domain features are slightly more developed and much more visible at this salt concentration (Figure 6D). The pores of the membrane are also larger in size. An SEM cross section image showed that the skin layer was less adherent to the substrate at 15000 ppm NaCl, compared to that at 2500 ppm NaCl (Supporting Information, Figure S4).

From the topography (Figure 6D), it is clear that the dissociation is restricted to surface layers (liquidlike) only. The inner layers are not disturbed by the salt ions where the re-formations are likely to take place. The transport data supported this observation as the percentage of rejection remained unaltered (Table 1). The re-formation processes take place easily in the nonlinear growing region where plenty of mobile chains are available for re-formation. However, the flux is compromised due to the thickness, which alters the separations. The thinner the skin layer, the better the performance of the membranes will be. Most suitable are a few bilayers that are sustainable in a linear growing region. The morphology confirmed this observation (Figure 6E), which shows complete restoration of the surface in the case of a mixed filtration of dye and salt. The presence of RB5 seems to have helped the re-formation process of the surface layers. Because the RB5 anion is tetravalent (Supporting Information, Figure S5), it can bind to four -NH_3^+ groups of CHI at a time, which means that RB5 can hold up to four different CHI repeating units (eq 3).

$$4\mathrm{Pol}^{+}\mathrm{Pol}^{-}{}_{(m)} + \mathrm{RB}^{4-}{}_{(aq)} + 4\mathrm{Na}^{+}{}_{(aq)} \rightleftharpoons (\mathrm{Pol}^{+})_4\mathrm{RB}^{4-}{}_{(m)} + 4\mathrm{Pol}^{-}\mathrm{Na}^{+}{}_{(m)} \quad (3)$$

where RB^{4-} represents the tetravalent RB5 anion. Moreover, the amino group present in RB5 exists as -NH_3^+, which can form ionic bonds with the carboxylate group of PAA. The possibility of secondary interactions such as hydrogen bonding between the amino and hydroxyl groups of RB5 with CHI could also facilitate the restoration process. The sustainability is obtained within a few nanometers (~50 nm) of the coating.

The observed morphological transformations are in complete agreement with the experimental values of flux and rejection presented in Table 1. As discussed earlier, salt intrusion weakens the polycation−polyanion interactions. Apparently, the polyelectrolyte chains break apart sufficiently to produce a more porous matrix, which accounts for the increase in flux. The increase in pore diameter obtained from the SEM images (Supporting Information, Table S2) also substantiates the increasing flux pattern at higher salt concentrations. The rejection of dye seems to have been mostly favored by the charge factor. Pore widening allowed for the appearance of dye molecules in the permeate, particularly at higher salt concentrations (74.5% at 10000 ppm NaCl, Table 1).

The filtration studies were also carried out at higher dye concentrations through CHI/PAA bilayers. The rejection and flux values are presented in Table 2. The increase in feed dye concentration to 500 ppm resulted in rejection of 98.64% with a flux of 25.79 $m^3\ m^{-2}\ day^{-1}$. Flux showed a decreasing trend

Table 2. Transport Characteristics of RB5 through a CHI/PAA Multilayer as a Function of the Number of Bilayers

RB5 feed concentration (ppm)	number of bilayers	NaCl feed concentration (ppm)	flux ($m^3\ m^{-2}\ day^{-1}$)	dye rejection (%)
500	4.5		37.92	60.47
	5.5		25.79	98.64
	6.5		4.85	98.99
	7.5		3.04	98.77
	9.5		0.10	99.72
	9.5	5000	1.18	97.69
	9.5	10000	2.33	98.41
1000	4.5		49.59	75.43
	5.5			76.19
	6.5		8.95	87.37
	7.5		3.81	
	9.5	5000	0.20	98.18
	9.5	10000	3.40	80.19

with additional layers of coating as expected. However, if the flux for a particular bilayer is compared at 100 and 500 ppm dye, flux is increased, which is enhanced further at even higher dye concentrations (Figure 7). This observation provides

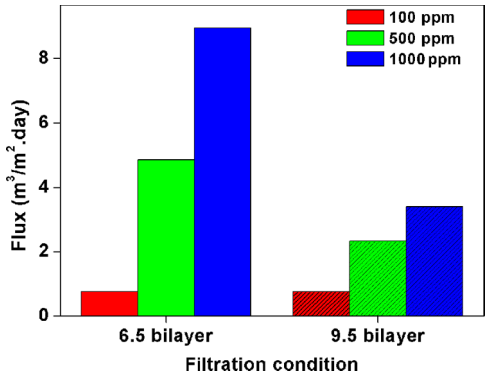

Figure 7. Variation of flux for 6.5 and 9.5 bilayers with respect to RB5 concentrations of 100, 500, and 1000 ppm. Shaded bars in the 9.5 bilayer experiment represent a feed solution containing 10000 ppm NaCl.

immediate support to the above discussion on the plasticizing action of RB5. Another outcome is that, at a concentration of 1000 ppm, a larger number of bilayers is necessary to reach a rejection percentage of 98.18. Because 9.5 bilayers are represented in the nonlinear growing region, flux is rather low. The addition of salt to the feed in this scenario also improves the flux value.

The morphological evaluation carried out for the 9.5 bilayer and the SEM images are given in Figure 8. A thick, porous morphology is observed, which transforms into more a porous network upon salt filtration. The surface morphological changes are altogether different. As expected, sustainability is maintained because re-formation takes place easily due to the presence of interdiffusing polymer chains. This observation is in agreement with that of Wang et al.,[31] who observed self-healing in a nonlinearly growing multilayer coating. The feature obtained at a higher electrolyte level (Figure 8 D) exhibited large, uniformly distributed pores with an average diameter of 1.74 μm. This may explain why it allows some dye to permeate.

DOI: 10.1021/am508298d
ACS Appl. Mater. Interfaces 2015, 7, 3699−3707

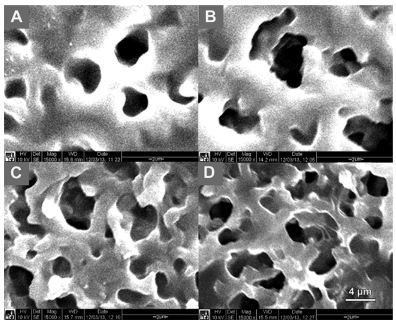

Figure 8. Morphological changes of a CHI/PAA 9.5 bilayer membrane (A) before exposure and after exposure to an RB5 solution containing (B) 0, (C) 5000, and (D) 10000 ppm NaCl.

Selectivity (α) for mixed salt/dye filtrations is a key parameter and is defined by Bruening et al.[10,51] as given in eq 4, where C_{perm} and C_{feed} are the solute concentrations in the permeate and feed, respectively, and R_A and R_B represent the percent rejection values of A (NaCl) and B (RB5), respectively.

$$\alpha = \frac{C_{A,perm}}{C_{A,feed}} \frac{C_{B,feed}}{C_{B,perm}} = \frac{100 - R_A}{100 - R_B} \quad (4)$$

For a particular set of membranes, selectivity is presented in Table 3. As the level of dye in the permeate was almost

Table 3. Salt/Dye Selectivity of the CHI/PAA Multilayers at a Salt Concentration of 5000 ppm in the Feed as a Function of the Number of Bilayers

number of bilayers	chloride rejection[a] (%)	RB5 rejection[b] (%)	selectivity[c]
5.5	15.25	99.99	8475
7.5	16.27	99.99	8373
8.5	16.30	99.99	8370
9.5	17.74	99.99	8226
10.5	18.33	99.99	8167

[a]Error bars ≤ ±4%. [b]Error bars ≤ ±0.01%. [c]Error bars ≤ ±50%.

negligible/extremely low, the values may carry some uncertainty. The observed selectivities are extremely high. The results presented here are following several repetitions of the experiment, and the passage of salt always remained >80%. Among the membranes studied, the best selectivity was observed for films loaded at 5000 ppm NaCl. The selectivity reported here is very high compared to those of commercial or multilayered membranes. Indeed, the experiments had to be run under dead end mode. However, to elaborate on the significance of the CHI/PAA surface further, desorption studies were carried out; the results are displayed in Figure 9. Both neutral and alkaline pH buffer solutions could retain the dye in buffered water though the alkaline pH (pH 10) seems to be more suitable. Time-dependent desorption studies indicated maximum unloading during the first 10 min. The dye adsorbed on the multilayer was desorbed by ∼80% within 30 min, which was increased to ∼85% by 60 min. The membranes were found to be reusable for the filtration of dye with an efficiency of 85 ± 5% after three adsorption−desorption cycles. This observation indicates that dye adsorption was primarily restricted to the surface layers, and that pores were comparatively free. The desorption trend also supported the feasibility of the process under steady state conditions. Images of the membranes during

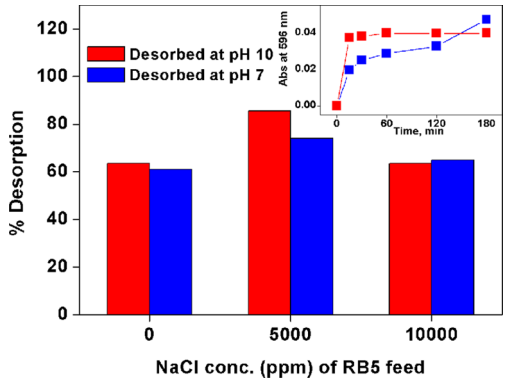

Figure 9. Extent of desorption of RB5 from a CHI/PAA 5.5 bilayer with respect to the buffered desorption solution pH and feed salt concentration. (inset) Time-dependent UV−vis absorbance (596 nm) of the buffer solution at pH 7 and 10 (the pH values at which RB5 is desorbed).

desorption are shown in Figure 10. Some initial experiments are also run with a local textile mill effluent. The results are

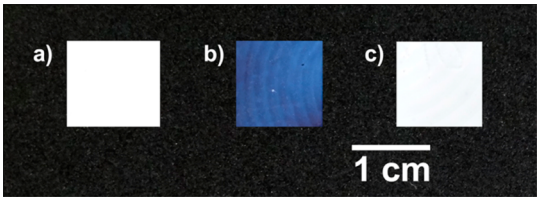

Figure 10. Digital photographs of a CHI/PAA 5.5 bilayer (a) before filtration, (b) after filtration with 100 ppm RB5, and (c) after desorption in buffer solution at pH 10.

Table 4. Percent Rejection of RB5 in Textile Effluent upon Low Pressure Filtration

pH of the textile effluent	dye rejection (%)
8.2	96.69 ± 0.2
3	98.77 ± 0.15

presented in Table 4. Preliminary data indicate reasonably good rejection. Further experiments are necessary to completely justify the suitability of a CHI/PAA multilayered membrane for industrial effluent treatment.

CONCLUSIONS

In summary, we show that the integrity of a membrane surface for industrial separations can be preserved by a few bilayers of coating. These nanolayers, though prone to variations in structure under stress, recover faster by making use of the same stress factor. This knowledge imparts new dimensions to asymmetric membrane structures for industrial purposes. This process is expected to be free of fouling because of the highly reversible nature of the LbL technique. The polyion pair used here is unique considering the economy and widespread availability of chitosan. It is anticipated that the concept of introducing sustainable surfaces will increase the lifespan of thin film coatings in many practical applications.

DOI: 10.1021/am508298d
ACS Appl. Mater. Interfaces 2015, 7, 3699−3707

■ ASSOCIATED CONTENT

Supporting Information

The degree of ionization of PAA in a CHI/PAA 5.5 bilayer, HPLC chromatogram of RB5 solution before and after filtration through a CHI/PAA 8.5 bilayer, the UV−vis absorbance spectra of RB5 permeate with respect to CHI/PAA multilayers, SEM images of CHI/PAA 5.5 bilayer membranes on filtration with various concentrations of NaCl solutions, SEM cross sectional images of CHI/PAA 5.5 bilayer membranes after filtration with 2500 and 15000 ppm NaCl solutions, structural formula of RB5, and average pore diameters of a CHI/PAA 5.5 bilayer after filtration with various salt solutions. This material is available free of charge via the Internet at http://pubs.acs.org.

■ AUTHOR INFORMATION

Corresponding Authors

*E-mail: ukaravind@gmail.com.
*E-mail: wiesner@duke.edu.

Notes

The authors declare no competing financial interest.

■ ACKNOWLEDGMENTS

The authors thank the Obama-Singh knowledge initiative (OSI) programme from the University Grants Commission (UGC) in New Delhi for financial support.

■ REFERENCES

(1) Allègre, C.; Moulin, P.; Maisseu, M.; Charbit, F. Treatment and Reuse of Reactive Dyeing Effluents. *J. Membr. Sci.* **2006**, *269*, 15−34.
(2) Koyuncu, I.; Topacik, D.; Yuksel, E. Reuse of Reactive Dyehouse Wastewater by Nanofiltration: Process Water Quality and Economical Implications. *Sep. Purif. Technol.* **2004**, *36*, 77−85.
(3) Vandevivere, P. C.; Bianchi, R.; Verstraete, W. Treatment and Reuse of Wastewater from the Textile Wet-processing Industry: Review of Emerging Technologies. *J. Chem. Technol. Biotechnol.* **1998**, *72*, 289−302.
(4) Lee, D.-K.; Cho, I.-C.; Lee, G.-S.; Kim, S.-C.; Kim, D.-S.; Yang, Y.-K. Catalytic Wet Oxidation of Reactive Dyes With H_2/O_2 Mixture on Pd−Pt/Al_2O_3 Catalysts. *Sep. Purif. Technol.* **2004**, *34*, 43−50.
(5) Baburaj, M. S.; Aravindakumar, C. T.; Sreedhanya, S.; Thomas, A. P.; Aravind, U. K. Treatment of Model Textile Effluents With PAA/CHI and PAA/PEI Composite Membranes. *Desalination* **2012**, *288*, 72−79.
(6) Sandhya, S.; Padmavathy, S.; Swaminathan, K.; Subrahmanyam, Y. V.; Kaul, S. N. Microaerophilic−Aerobic Sequential Batch Reactor for Treatment of Azo Dyes Containing Simulated Wastewater. *Process Biochem. (Oxford, U.K.)* **2005**, *40*, 885−890.
(7) Blackburn, R. S. Natural Polysaccharides and Their Interactions with Dye Molecules: Applications in Effluent Treatment. *Environ. Sci. Technol.* **2004**, *38*, 4905−4909.
(8) Erswell, A.; Brouckaert, C. J.; Buckley, C. A. The Reuse of Reactive Dye Liquors Using Charged Ultrafiltration Membrane Technology. *Desalination* **1988**, *70*, 157−167.
(9) Banat, I. M.; Nigam, P.; Singh, D.; Marchant, R. Microbial Decolorization of Textile-Dye Containing Effluents: A Review. *Bioresour. Technol.* **1996**, *58*, 217−227.
(10) Hong, S. U.; Miller, M. D.; Bruening, M. L. Removal of Dyes, Sugars, and Amino Acids from NaCl Solutions Using Multilayer Polyelectrolyte Nanofiltration Membranes. *Ind. Eng. Chem. Res.* **2006**, *45*, 6284−6288.
(11) Hammond, P. T. Form and Function in Multilayer Assembly: New Applications at the Nanoscale. *Adv. Mater. (Weinheim, Ger.)* **2004**, *16*, 1271−1293.
(12) Ariga, K.; Hill, J. P.; Ji, Q. Layer-by-layer Assembly as a Versatile Bottom-up Nanofabrication Technique for Exploratory Research and Realistic Application. *Phys. Chem. Chem. Phys.* **2007**, *9*, 2319−2340.
(13) Ghostine, R. A.; Jisr, R. M.; Lehaf, A.; Schlenoff, J. B. Roughness and Salt Annealing in a Polyelectrolyte Multilayer. *Langmuir* **2013**, *29*, 11742−11750.
(14) Cho, Y.; Lim, J.; Char, K. Layer-by-layer Assembled Stimuli-Responsive Nanoporous Membranes. *Soft Matter* **2012**, *8*, 10271−10278.
(15) Gong, X.; Han, L.; Gao, J.; Gao, C. Stability of Polyelectrolyte Multilayer Micropatterns in Response to Post-Treatments. *Colloids Surf., A* **2012**, *396*, 299−304.
(16) Antipov, A. A.; Sukhorukov, G. B.; Möhwald, H. Influence of the Ionic Strength on the Polyelectrolyte Multilayers' Permeability. *Langmuir* **2003**, *19*, 2444−2448.
(17) McAloney, R. A.; Dudnik, V.; Goh, M. C. Kinetics of Salt-Induced Annealing of a Polyelectrolyte Multilayer Film Morphology. *Langmuir* **2003**, *19*, 3947−3952.
(18) Choi, J.; Rubner, M. F. Influence of the Degree of Ionization on Weak Polyelectrolyte Multilayer Assembly. *Macromolecules* **2005**, *38*, 116−124.
(19) Shiratori, S. S.; Rubner, M. F. pH-Dependent Thickness Behavior of Sequentially Adsorbed Layers of Weak Polyelectrolytes. *Macromolecules* **2000**, *33*, 4213−4219.
(20) Guzman, E.; Ritacco, H.; Rubio, J. E. F.; Rubio, R. G.; Ortega, F. Salt-induced Changes in the Growth of Polyelectrolyte Layers of Poly(diallyl-dimethylammonium chloride) and Poly(4-styrene sulfonate of sodium). *Soft Matter* **2009**, *5*, 2130−2142.
(21) Peyratout, C. S.; Dähne, L. Tailor-Made Polyelectrolyte Microcapsules: From Multilayers to Smart Containers. *Angew. Chem., Int. Ed.* **2004**, *43*, 3762−3783.
(22) Decher, G.; Hong, J.-D. Buildup of Ultrathin Multilayer Films by a Self-Assembly Process, 1 Consecutive Adsorption of Anionic and Cationic Bipolar Amphiphiles on Charged Surfaces. *Makromol. Chem., Macromol. Symp.* **1991**, *46*, 321−327.
(23) Santos, D. E. S.; Neto, C. G. T.; Fonseca, J. L. C.; Pereira, M. R. Chitosan Macroporous Asymmetric Membranes−Preparation, Characterization and Transport of Drugs. *J. Membr. Sci.* **2008**, *325*, 362−370.
(24) Li, X. Y.; Nan, K. H.; Chen, H.; Xu, Y. Preparation and Characterization of Chitosan Nanopores Membranes for the Transport of Drugs. *Int. J. Pharm.* **2011**, *420*, 371−377.
(25) Guzman, E.; Chuliá-Jordán, R.; Ortega, F.; Rubio, R. G. Influence of the Percentage of Acetylation on the Assembly of LbL Multilayers of Poly(acrylic acid) and Chitosan. *Phys. Chem. Chem. Phys.* **2011**, *13*, 18200−18207.
(26) Guzman, E.; Cavallo, J. A.; Chuliá-Jordán, R.; Gómez, C.; Strumia, M. C.; Ortega, F.; Rubio, R. G. pH-Induced Changes in the Fabrication of Multilayers of Poly(acrylic acid) and Chitosan: Fabrication, Properties, and Tests as a Drug Storage and Delivery System. *Langmuir* **2011**, *27*, 6836−6845.
(27) Barthlott, W.; Neinhuis, C. Purity of the Sacred Lotus, or Escape from Contamination in Biological Surfaces. *Planta* **1997**, *202*, 1−8.
(28) Neinhuis, C.; Barthlott, W. Characterization and Distribution of Water-Repellent, Self-Cleaning Plant Surfaces. *Ann. Bot. (Oxford, U.K.)* **1997**, *79*, 667−677.
(29) Li, Y.; Li, L.; Sun, J. Bioinspired Self-Healing Superhydrophobic Coatings. *Angew. Chem., Int. Ed.* **2010**, *49*, 6129−6133.
(30) Zhai, L.; Berg, M. C.; Cebeci, F. Ç.; Kim, Y.; Milwid, J. M.; Rubner, M. F.; Cohen, R. E. Patterned Superhydrophobic Surfaces: Toward a Synthetic Mimic of the Namib Desert Beetle. *Nano Lett.* **2006**, *6*, 1213−1217.
(31) Wang, X.; Liu, F.; Zheng, X.; Sun, J. Water-Enabled Self-Healing of Polyelectrolyte Multilayer Coatings. *Angew. Chem., Int. Ed.* **2011**, *50*, 11378−11381.
(32) Shchukin, D. G.; Zheludkevich, M.; Yasakau, K.; Lamaka, S.; Ferreira, M. G. S.; Möhwald, H. Layer-by-Layer Assembled Nanocontainers for Self-Healing Corrosion Protection. *Adv. Mater. (Weinheim, Ger.)* **2006**, *18*, 1672−1678.

DOI: 10.1021/am508298d
ACS Appl. Mater. Interfaces 2015, 7, 3699−3707

(33) Chen, Y.; He, F.; Ren, Y.; Peng, H.; Huang, K. Fabrication of Chitosan/PAA Multilayer onto Magnetic Microspheres by LbL Method for Removal of Dyes. *Chem. Eng. J. (Amsterdam, Neth.)* **2014**, *249*, 79−92.
(34) Rinaudo, M.; Pavlov, G.; Desbrières, J. Solubilization of Chitosan in Strong Acid Medium. *Int. J. Polym. Anal. Charact.* **1999**, *5*, 267−276.
(35) Rinaudo, M.; Pavlov, G.; Desbrières, J. Influence of Acetic Acid Concentration on the Solubilization of Chitosan. *Polymer* **1999**, *40*, 7029−7032.
(36) Disha, V. J.; Aravindakumar, C. T.; Aravind, U. K. Phosphate Recovery by High Flux Low Pressure Multilayer Membranes. *Langmuir* **2012**, *28*, 12744−12752.
(37) Aravind, U. K.; Mathew, J.; Aravindakumar, C. T. Transport Studies of BSA, Lysozyme and Ovalbumin through Chitosan/Polystyrene Sulfonate Multilayer Membrane. *J. Membr. Sci.* **2007**, *299*, 146−155.
(38) Aravind, U. K.; George, B.; Baburaj, M. S.; Thomas, S.; Thomas, A. P.; Aravindakumar, C. T. Treatment of Industrial Effluents Using Polyelectrolyte Membranes. *Desalination* **2010**, *252*, 27−32.
(39) Mathew, J.; Sreedhanya, S.; Baburaj, M. S.; Aravindakumar, C. T.; Aravind, U. K. Fabrication of Switchable Protein Resistant and Adhesive Multilayer Membranes. *Colloids Surf., B* **2012**, *94*, 118−124.
(40) Guzman, E.; San Miguel, V.; Peinado, C.; Ortega, F.; Rubio, R. G. Polyelectrolyte Multilayers Containing Triblock Copolymers of Different Charge Ratio. *Langmuir* **2010**, *26*, 11494−11502.
(41) Rubio, A. M.; Freire, J. J.; Horta, A.; Depierola, I. F. Influence of Long-Range Interactions on the End-to-End Distance Distribution and Cyclization Probability of Short Chains. *Macromolecules* **1991**, *24*, 5167−5170.
(42) Itano, K.; Choi, J.; Rubner, M. F. Mechanism of the pH-Induced Discontinuous Swelling/Deswelling Transitions of Poly(allylamine hydrochloride)-Containing Polyelectrolyte Multilayer Films. *Macromolecules* **2005**, *38*, 3450−3460.
(43) Xie, A. F.; Granick, S. Local Electrostatics within a Polyelectrolyte Multilayer with Embedded Weak Polyelectrolyte. *Macromolecules* **2002**, *35*, 1805−1813.
(44) Liu, C.; Thormann, E.; Claesson, P. M.; Tyrode, E. Surface Grafted Chitosan Gels. Part II. Gel Formation and Characterization. *Langmuir* **2014**, *30*, 8878−8888.
(45) Bieker, P.; Schönhoff, M. Linear and Exponential Growth Regimes of Multilayers of Weak Polyelectrolytes in Dependence on pH. *Macromolecules* **2010**, *43*, 5052−5059.
(46) Lavalle, P.; Picart, C.; Mutterer, J.; Gergely, C.; Reiss, H.; Voegel, J.-C.; Senger, B.; Schaaf, P. Modeling the Buildup of Polyelectrolyte Multilayer Films Having Exponential Growth. *J. Phys. Chem. B* **2004**, *108*, 635−648.
(47) Haynie, D. T.; Cho, E.; Waduge, P. "In and Out Diffusion" Hypothesis of Exponential Multilayer Film Buildup Revisited. *Langmuir* **2011**, *27*, 5700−5704.
(48) Guzmán, E.; Ritacco, H. A.; Ortega, F.; Rubio, R. G. Growth of Polyelectrolyte Layers Formed by Poly(4-styrenesulfonate sodium salt) and Two Different Polycations: New Insights from Study of Adsorption Kinetics. *J. Phys. Chem. C* **2012**, *116*, 15474−15483.
(49) Liu, C.; Thormann, E.; Claesson, P. M.; Tyrode, E. Surface Grafted Chitosan Gels. Part I. Molecular Insight into the Formation of Chitosan and Poly(acrylic acid) Multilayers. *Langmuir* **2014**, *30*, 8866−8877.
(50) Nolte, A. J.; Takane, N.; Hindman, E.; Gaynor, W.; Rubner, M. F.; Cohen, R. E. Thin Film Thickness Gradients and Spatial Patterning via Salt Etching of Polyelectrolyte Multilayers. *Macromolecules* **2007**, *40*, 5479−5486.
(51) Liu, X. Y.; Bruening, M. L. Size-Selective Transport of Uncharged Solutes through Multilayer Polyelectrolyte Membranes. *Chem. Mater.* **2004**, *16*, 351−357.

DOI: 10.1021/am508298d
ACS Appl. Mater. Interfaces 2015, 7, 3699−3707